Korean J. Chem. Eng., 33(5), 1557-1564 (2016)
DOI: 10.1007/s11814-016-0005-x

pISSN: 0256-1115
eISSN: 1975-7220

Heterogeneous Fenton degradation of Orange II by immobilization of Fe_3O_4 nanoparticles onto Al-Fe pillared bentonite

Wenbing Li*,,†, Dong Wan*,†, Guanghua Wang*,**, Kun Chen*, Qin Hu*, and Lulu Lu***

*College of Chemical Engineering and Technology, Wuhan University of Science and Technology, Wuhan 430081, China
**Hubei Coal Conversion and New Carbon Materials Key Laboratory, Wuhan 430081, China
(*Received 28 November 2014 • accepted 4 January 2016*)

Abstract−A novel catalyst, Fe_3O_4 nanoparticle decorated Al-Fe pillared bentonite (Fe_3O_4/Al-Fe-P-B), was prepared by in situ precipitation oxidization method. The catalyst was characterized by SEM, XRD and Raman spectroscopy. The Fe_3O_4 nanoparticles mainly exist on the surface or enter into the pore of bentonite, with better dispersing and less coaggregation. The catalytic activity of Fe_3O_4/Al-Fe-P-B was investigated in the degradation of Orange II (OII) by heterogeneous Fenton-like process. The effects of initial concentration of hydrogen peroxide, catalyst loading, temperature and initial pH on the degradation of OII were investigated. The Fe_3O_4/Al-Fe-P-B showed higher degradation efficiency of OII than bare Fe_3O_4 or Al-Fe-P-B in the degradation experiment. The enhanced catalytic activity of Fe_3O_4/Al-Fe-P-B in heterogeneous Fenton system was due to the synergistic effect between Al-Fe-P-B and Fe_3O_4. The novel catalyst can achieve solid-liquid separation easily by sample magnetic separation and has a good reusability and stability.

Keywords: Magnetic Bentonite, Heterogeneous Catalyst, Degradation, Orange II, Magnetic Separation

INTRODUTION

Fenton and Fenton-like technology have been extensively studied as one of the best options for the degradation of various recalcitrant organic pollutants in water. However, there is a non-ignorable drawback of traditional homogeneous Fenton that it is difficult to remove the iron sludge after the treatment and may cause secondary pollution [1,2]. Recently, heterogeneous Fenton-like systems using solid catalysts have been developed. Most of the researches on heterogeneous Fenton-like catalysts have been focused on iron supported materials, such as zero valent iron (Fe^0) [3], iron-based clays [4] and iron oxide minerals [5]. Among these catalysts, iron oxide minerals, especially magnetite (Fe_3O_4) nanoparticles, attracted more attention, since Fe_3O_4 contains both Fe^{2+} and Fe^{3+}, which are the crucial cations for initiation of Fenton reaction according to the classical Haber-Weiss mechanism [6]. Moreover, with an inverse spinel crystal structure, the electrons can transfer between Fe^{2+} and Fe^{3+} in the octahedral sites, allowing the Fe species to be reversibly oxidized and reduced while keeping the same structure [7]. In addition, Fe_3O_4 nanoparticles are magnetic and can be easily separated from the terminal solution by magnetic separation.

With the advantages of strong catalytic activity, long-term stability, excellent environment-friendly and, especially, the intrinsic peroxidase-like activity [6], Fe_3O_4 nanoparticles are investigated as ideal heterogeneous Fenton-like catalysts for the removal of environmental contaminants, including phenol [7], aniline [8], 2,4-dichlorophenol [9], p-nitrophenol [10] and dye pollutants [11]. However, the coaggregation of Fe_3O_4 nanoparticles often constitutes a challenge that nanomaterials have to be confronted, since the coaggregation decreases the effective surface active sites of nanoparticles and thus reduces their catalytic activities, especially in water solution [12]. Several methods have been accordingly developed for overcoming the coaggregation of nanoparticles. Recently, immobilized Fe_3O_4 nanoparticles on solid supports during the preparation process were found to be effective to prevent coaggregation and improve the catalytic activity. The supports can be organic and inorganic materials, such as activated carbon [13], multiwalled carbon nanotubes [14], mesocellular carbon foam [15] and poly(3,4-ethylenedioxythiophene) [16]. It is well accepted that the supporting materials must be of high stability, low cost and environmental harmony.

Bentonite is a kind of natural 2 : 1 type layered clay mineral with high stability, microporosity, larger surface area and low cost that has been widely used in a number of industrial branches [17]. After intercalating by polymeric inorganic oxocations, the stability, surface area and catalytic performance of bentonite could be promoted effectively [18]. Many researches on intercalated bentonite have been focused on Al-Fe pillared bentonite, which could be used as a heterogeneous Fenton-like catalyst [19-21]. With so many excellent properties, pillared bentonite may be particularly suitable as a support for the synthesis of magnetic nanoparticles. Thus, immobilizing Fe_3O_4 nanoparticles on Al-Fe pillared bentonite may have some advantages. On one hand, the coaggregation of Fe_3O_4 nanoparticles could be prevented effectively. On the other hand, the Al-Fe pillared bentonite may achieve solid-liquid separation easily by magnetic separation technology. The most important is that there may be a synergistic effect between the Al-Fe pillared bentonite and Fe_3O_4 nanoparticles, which can improve the catalytic activity of the catalyst. However, so far, few attempts to synthesize pillared bentonite-supported Fe_3O_4 composite could be found in literatures, and the magnetic bentonite was mainly prepared to act as adsorbent instead

†To whom correspondence should be addressed.
E-mail: wandongchn@126.com, liwenbing@126.com

of heterogeneous Fenton-like catalyst [22-26]. Since the mimic enzyme catalysis process is becoming a novel challenging field and a hot area of research in the green chemical engineering, it is urgent to develop a low cost, environment-friendly and high-efficiency heterogeneous catalyst to meet the needs of environmental protection.

In our previous research, we used Al-pillared bentonite to immobilize Fe_3O_4 nanoparticles by in situ co-precipitation method (c-Fe_3O_4) [27]. The average size of Fe_3O_4 nanoparticles was around 20-25 nm. However, in this post-study survey, we found that Fe_3O_4 nanoparticles with diameter ranging from 40 to 100 nm, synthesized through precipitation oxidization method (o-Fe_3O_4), had higher catalytic performance and stability, which can be seen from Fig. S1 and Fig. S2 in supplementary data. From the XRD patterns of these two kinds of Fe_3O_4 nanoparticles (Fig. S3), we can find that the o-Fe_3O_4 has higher crystallinity than c-Fe_3O_4. It is the higher crystallinity and Fe^{II}/Fe^{III} ratio that give o-Fe_3O_4 better oxidation efficiency for dye removal. Similar results were also found by Xue et al. [28]. On the other hand, Al-Fe pillared bentonite showed higher adsorption and catalytic performance than Al pillared bentonite [21]. Thus, we propose a new strategy toward Al-Fe pillared bentonite-supported Fe_3O_4 nanoparticles (Fe_3O_4/Al-Fe-P-B). The nanocomposites were prepared through in situ precipitation oxidization method for the first time and further used for the removal of organic pollutants in water. As known, Orange II(OII) is a typical azo dye and has been selected as a model dyeing pollutant in many investigations because of its widespread application and recalcitrant nature [4,21,29]. To evaluate the feasibility of the prepared nanocomposites to be used as heterogeneous Fenton-like catalyst in the organic wastewater treatment, Orange II was selected as the target pollutant. The reaction conditions of Orange II in the Fenton processes in the presence of nanocomposites were optimized. The microstructure, morphology and stability of the nanocomposites were also investigated.

MATERIALS AND METHODS

1. Materials

Natural bentonite was procured from Shanghai No. 4 Reagent & H.V. Chemical Co., Ltd., China. Orange II(OII) was obtained from Shanghai Zhanyun Chemical Co., Ltd., China. All chemicals were of analytical grade and used as received. In the experiments, distilled water was used for preparing the solutions and suspensions.

2. Preparation of Fe_3O_4/Al-Fe-P-B Catalyst

The Al-Fe pillared bentonite (Al-Fe-P-B) was prepared by pillaring the bentonite through cation-exchange process as described in the literature [21]. The nanocomposites were synthesized by in situ precipitation oxidization method. 2 g Al-Fe-P-B was added into a 500 mL flask containing 200 mL distilled water with constantly stirring. The solution was bubbled with N_2 flow for 15 min to remove the dissolved oxygen and placed in a 95 °C water bath, and then 8 g $FeSO_4 \cdot 7H_2O$ and 3.6 g $NaNO_3$ were added into the flask. Afterwards, 40 mL ammonia was added dropwise (2 mL min^{-1}) into the heating solution while keeping vigorous stirring and stable N_2 flow during the entire reaction period. After that, the solution was heated at 95 °C for another hour, and then cooled to room temperature. The precipitate was isolated by a permanent magnet. After repeated washing with deionized water and absolute ethanol under ultrasonication, the formed Fe_3O_4/Al-Fe-P-B nanocomposites were dried in a vacuum oven at 100 °C for 12 h. Fe_3O_4 was synthesized as above procedure without adding Al-Fe-P-B. All the products were stored in a desiccator under ambient temperature for further experiments.

3. Characterization

X-ray diffraction (XRD) patterns of the samples were recorded by a Rigaku D/max-RB diffractometer (Rigaku, Japan) at 40 kV and 30 mA using filtered Cu Kα radiation (λ=0.15418 nm). Raman spectra were obtained using the DXR laser micro-Raman spectrometer (Thermo Scientific, America) at a laser wavelength of 780 nm. Micrographs of the samples were taken using a Nova400 Nano SEM (FEI, America). Before observation of SEM, all samples were fixed on silicon wafer and coated with gold.

4. Degradation of Orange II by Heterogeneous Fenton Experiments

The experiments were carried out in a conical flask with a stopper (containing 200 mL of reaction solution). The dosage of catalyst was 0-2.0 g L^{-1} while the concentrations of OII and H_2O_2 were 0.23 mmol L^{-1} and 0-25 mmol L^{-1}, respectively. All experiments were carried out under constant stirring to make good catalyst dispersion. The initial pH of solution was adjusted by H_2SO_4 and NaOH. Before reaction, the suspension containing catalyst and OII was stirred for 60 min to achieve adsorption equilibrium. A 1-mL sample was withdrawn from the reactor to analyze the decolorization efficiency of 0 min. The Fenton reaction was initiated when H_2O_2 was added to the OII solution. After the oxidation reaction, the catalyst was repeated washing and dried for reusing.

5. Analyses

At given intervals of degradation, a sample was analyzed by UV-Vis spectroscopy (Ultrospec 3300 pro, GE Healthcare Bio-Sciences China Ltd.) at a wavelength of 484 nm, which is the maximum absorption wavelength of Orange II [4]. The concentration of Orange II was converted through the standard curve method of dyes. The concentration of Fe^{2+} and total iron concentration (ΣFe^{n+}) in the solution was measured by the 1,10-phenatroline spectrophotometric method [29]. The chemical oxygen demand (COD_{Cr}) was determined by dichromate method. To eliminate the interference of H_2O_2 with COD_{Cr} measurements, the reaction was finally blocked by raising the pH to 9-10, adding MnO_2 and allowing the samples to sit overnight [30].

RESULTS AND DISCUSSION

1. Characterization of Catalyst

The morphologies of pillared bentonite and catalysts were characterized by SEM. The SEM images in Fig. 1(a) show that the pillared bentonite is layer structure and has a coarse porous surface. The synthesized Fe_3O_4 (Fig. 1(b)) are spherical-like mostly and dramatically co-aggregated together, while in the sample of Fe_3O_4/Al-Fe-P-B (Fig. 1(c)), the supported Fe_3O_4 nanoparticles exist on the surface or enter into the pore of bentonite, with better dispersing and less co-aggregation. Besides, the N_2 adsorption-desorption isotherms for Fe_3O_4 and Fe_3O_4/Al-Fe-P-B were also recorded, which

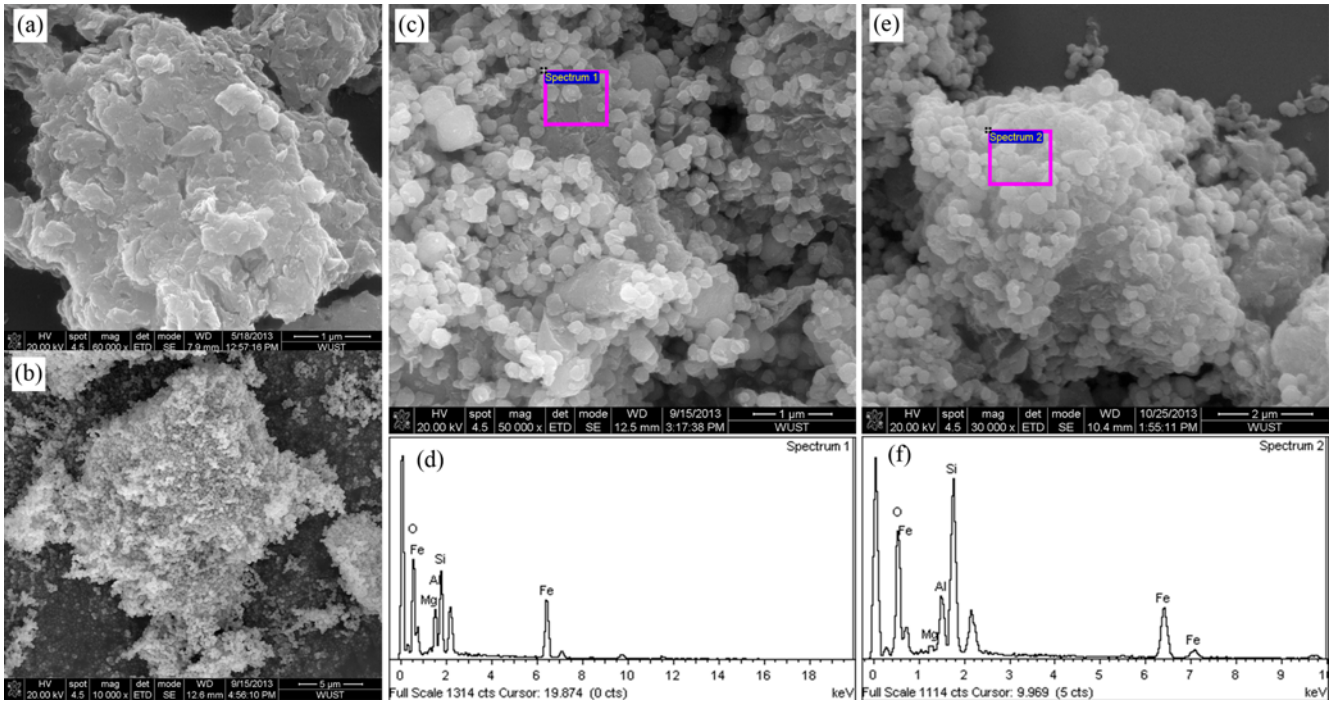

Fig. 1. SEM photograph of Al-Fe-P-B (a), Fe_3O_4 (b), Fe_3O_4/Al-Fe-P-B (c) and reused Fe_3O_4/Al-Fe-P-B (e) and EDS spectra of Fe_3O_4/Al-Fe-P-B (d) and reused Fe_3O_4/Al-Fe-P-B (f).

is shown in Fig. S4 in supplementary data. The specific surface areas calculated by using a BET equation are found to be 4.68 and 53.02 $m^2 g^{-1}$ for Fe_3O_4 and Fe_3O_4/Al-Fe-P-B, respectively. And wide hysteresis area of N_2 adsorption/desorption isotherms can be clearly seen in the case of Fe_3O_4/Al-Fe-P-B, suggesting the wide distributions of pores in the nanocomposites. Although the products have experienced repeated washing in water and methanol under ultrasonication before SEM measurements, almost all magnetite nanoparticles are still found on the bentonite surface. This indicates the strong interaction between Al-Fe-P-B and magnetite nanoparticles. The diameter of Fe_3O_4 nanoparticles ranges from 40 to 100 nm. The EDS spectra of Fe_3O_4/Al-Fe-P-B are shown in Fig. 1(d). It can be found that the nanocomposite mainly consists of O, Si, Al, Mg and Fe. The image of Fe_3O_4/Al-Fe-P-B nanoparticles reused for three times in Fig. 1(e) shows no obvious change of structure of the catalyst after oxidation reaction. The saturation magnetization of Fe_3O_4/Al-Fe-P-B is 30.9 emu g^{-1}, which can be seen in Fig. S5 in supplementary data. Such a high magnetization makes the nanocomposite be quickly separated from its dispersion with a magnet.

The X-ray diffraction patterns of the samples are shown in Fig. 2(a). Diffraction peaks assigned to bentonite at 2θ=5.5° [17,18] can be seen for Al-Fe-P-B and Fe_3O_4/Al-Fe-P-B nanocomposites, indicating that the bentonite structure is not destroyed after treatment by pillaring process and the chemical precipitation of Fe_3O_4. As shown in Fig. 2(a), eight characteristic peaks for Fe_3O_4 (2θ=18, 30, 35.5, 37, 43, 53.4, 57 and 62.5) are observed for the synthesized Fe_3O_4 and Fe_3O_4/Al-Fe-P-B nanocomposites. And no other peaks corresponding to the hematite are detected in the XRD patterns, indicating that the Fe_3O_4 nanoparticles in the composites are pure Fe_3O_4 with inverse spinel structure [31].

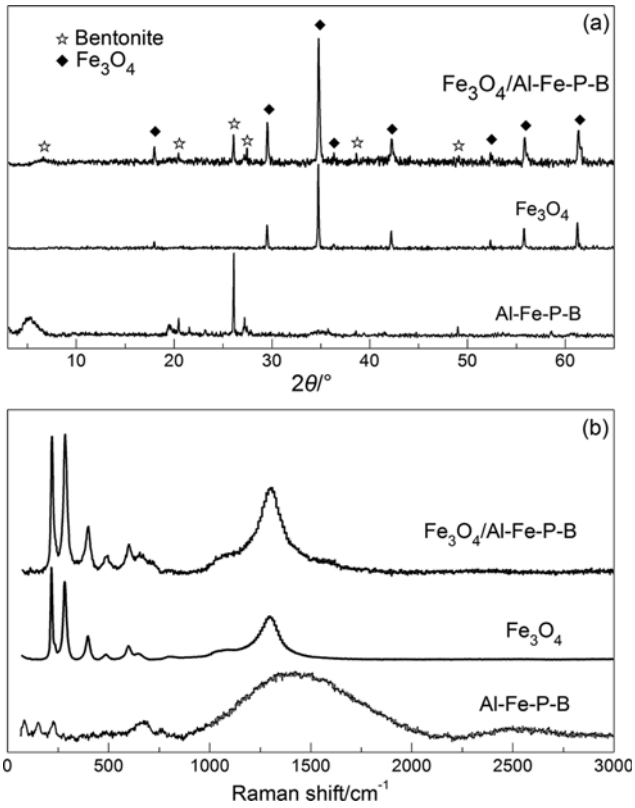

Fig. 2. XRD patterns (a) and Raman spectra (b) of the samples.

Fig. 2(b) shows the Raman spectra of the samples. The peak found at 152 cm^{-1} is attributed to the O-Al-O symmetric bending

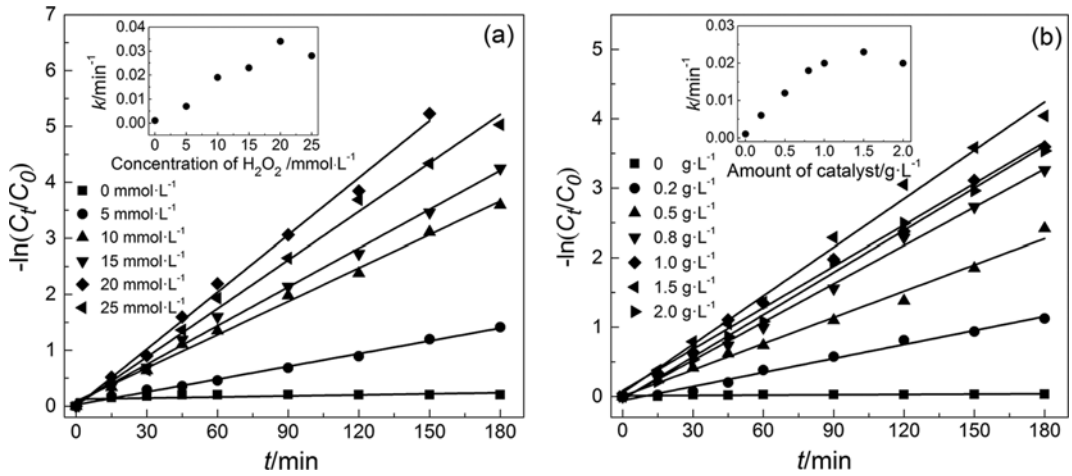

Fig. 3. The effects of H_2O_2 concentration (a) and amount of catalyst (b) on the degradation efficiency of Orange II. Inset: correlation of the apparent pseudo-first-order rate constant (C_{OII}=0.23 mmol·L^{-1}, 1.0 g·L^{-1} of catalyst, 10 mmol·L^{-1} of H_2O_2, pH=3.5, 40 °C).

mode of the AlO_6 octahedron. The band at 704 cm^{-1} can be assigned to the symmetric stretching of the Si-O-Si group in the SiO_4 tetrahedral layer of the phyllosilicates [32]. The bands at 232, 299, 410, 501 and 615 cm^{-1} are characteristic peaks of Fe_3O_4 [33], which are also found in the Raman spectra of Fe_3O_4/Al-Fe-P-B. It is in conformity with the XRD analysis.

2. Catalytic Performance of Catalysts

2-1. Effect of the Hydrogen Peroxide Concentration

The effect of hydrogen peroxide was analyzed by varying its initial concentration between 0 mmol L^{-1} and 25 mmol L^{-1} (Fig. 3(a)). Under all tested conditions, the OII degradation was observed to approximately follow a pseudo-first-order reaction in kinetics, which can be expressed as $-\ln(C_t/C_0)=kt$, where C_0 and C_t (mg·L^{-1}) is the concentration of OII at 0 min and t min, k (min^{-1}) is the apparent pseudo-first-order rate constant and t (min) is the reaction time. The k constants were obtained from the slopes of the straight lines by plotting $-\ln(C_t/C_0)$ as a function of time t, through regression [34]. Good correlation coefficients (R^2>0.98) are obtained in our systems. From Fig. 3(a) there is little OII removed in the absence of H_2O_2. According to the previous study, 42 mol of H_2O_2 was theoretically needed for complete degradation of 1 mol of the dye:

$$C_{16}H_{11}N_2SO_4Na+42H_2O_2 \rightarrow 16CO_2+46H_2O+2HNO_3+NaHSO_4 \quad (1)$$

Based on this equation, the necessary amount of H_2O_2 in the present study for complete degradation of 100 mg L^{-1} (0.23 mmol L^{-1}) of OII is 9.54 mmol L^{-1}. It is observed that the degradation rate of OII increases observably when H_2O_2 concentration increases from 0 to 10 mmol L^{-1}. Since the OII degradation is directly related to the concentration of the •OH produced by the catalytic decomposition of H_2O_2, more OII decomposition is expected with a higher H_2O_2 concentration. However, a significant improvement is not seen when the H_2O_2 concentration increased to 15 mmol L^{-1}, which can be explained by the scavenging effect of •OH by H_2O_2:

$$H_2O_2+\bullet OH \rightarrow H_2O+\bullet OOH \quad (2)$$

The oxidation potential of •OOH is much smaller than that of the •OH species. Therefore, it makes the reaction slow down though the rate constant still increases. However, when the H_2O_2 concentration increases to 20 mmol L^{-1}, the degradation process turns to significantly accelerate. The main reason for this phenomenon may be that the increase of H_2O_2 dosage increases the dissolved iron concentration under acid condition and induces the homogeneous catalytic oxidation. The rate constant is reduced slightly at a much higher H_2O_2 concentration (25 mmol L^{-1}), due to the accelerating of the Eq. (2).

2-2. Effect of Catalyst Dosage

As expected, OII degradation rate increases dramatically as the amount of employed catalyst increases from 0 to 1.0 g L^{-1} (Fig. 3(b)), due to the increasing amount of active sites for the formation of •OH and, maybe equally important, for OII adsorption. Nevertheless, when catalyst addition is further increased to 2.0 g L^{-1}, the degradation of OII does not enhance but slightly decreases, because of the agglomeration of nanoparticles and the scavenging of hydroxyl radicals or other radicals by present iron species through undesirable reactions (3)-(5) [9].

$$Fe^{2+}+\bullet OH \rightarrow OH^-+Fe^{3+} \quad (3)$$

$$Fe^{2+}+\bullet OOH \rightarrow OOH^-+Fe^{3+} \quad (4)$$

$$Fe^{3+}+\bullet OOH \rightarrow Fe^{2+}+O_2+H^+ \quad (5)$$

2-3. Effect of Temperature

The degradation efficiency of OII increases with the increase of temperature, as seen from Fig. 4. According to previous study [4], the change in enthalpy that follows the oxidative degradation of OII is positive while the process is endothermic. Accordingly, the increase of the reaction temperature is beneficial for the degradation of OII solutions. In addition, the k constant at different temperatures can be expressed by the Arrhenius equation as follows:

$$k=A\times\exp(-E_a/RT) \quad (6)$$

where k is the rate constant, A is a pre-exponential factor, E_a is reaction activation energy (kJ mol^{-1}), R is the gas constant (8.314 J mol^{-1} K^{-1}), and T is the absolute temperature (K). According to the equation, we have

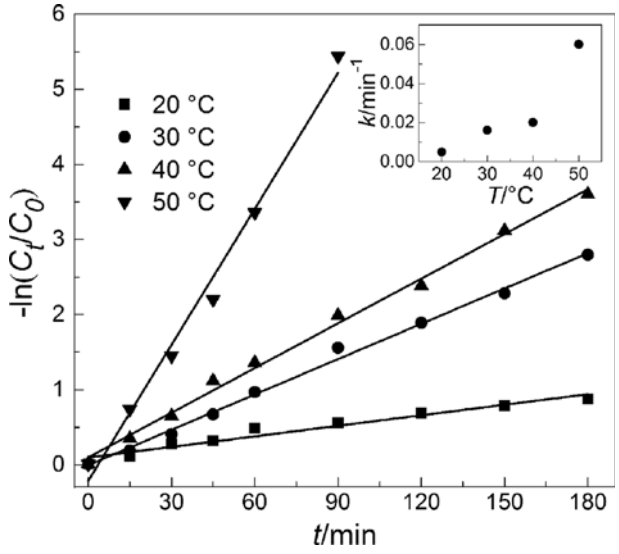

Fig. 4. The effect of temperature on the degradation efficiency of Orange II. Inset: correlation of the apparent pseudo-first-order rate constant with temperature (C_{OII}=0.23 mmol·L^{-1}, 10 mmol·L^{-1} of H_2O_2, 1.0 g·L^{-1} of catalyst, pH=3.5).

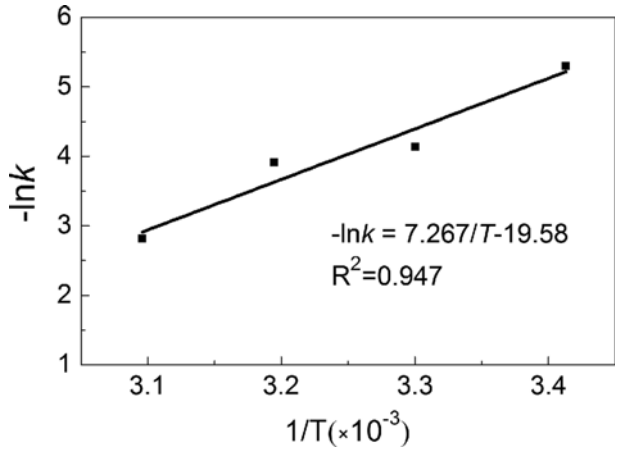

Fig. 5. Arrhenius plots for degradation of Orange II catalyzed by magnetic bentonite.

$$-\ln k = E_a/RT - \ln A \quad (7)$$

In terms of the data in Fig. 4, by plotting lnk versus 1/T, we obtained the E_a value from the slope of the straight line (Fig. 5). The E_a value calculated is 60.42 kJ mol^{-1}, which is similar to the result reported earlier [34].

2-4. Effect of Initial pH

The effect of initial solution pH on the degradation rate of OII is shown in Fig. 6. When the initial pH is 3.0, OII can be quickly degraded in 120 min under the adopted conditions. But as the initial pH rises, the degradation becomes much slower. The increased degradation efficiency at lower pH values can be attributed to the higher oxidation potential of hydroxyl radicals, whose generation rate is enhanced in a lower pH value [14]. The previous studies approved that lower pH could increase the electrostatic attraction

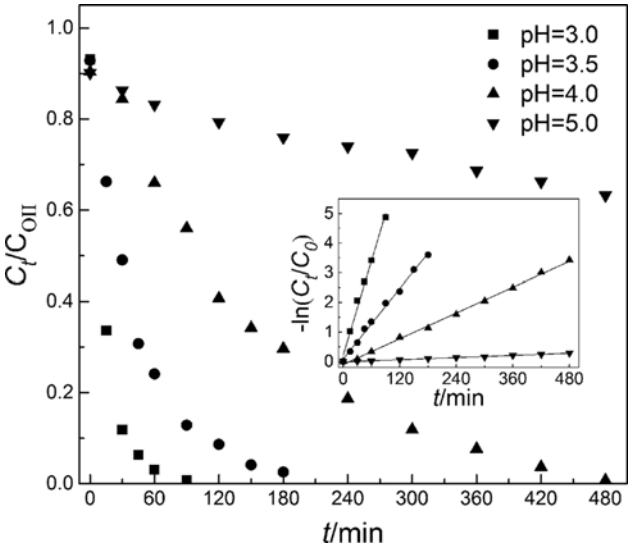

Fig. 6. The effect of initial pH on the degradation efficiency of Orange II. Inset: fitted by pseudo-first-order rate law (C_{OII}=0.23 mmol·L^{-1}, 10 mmol·L^{-1} of H_2O_2, 1.0 g·L^{-1} of catalyst, 40 °C).

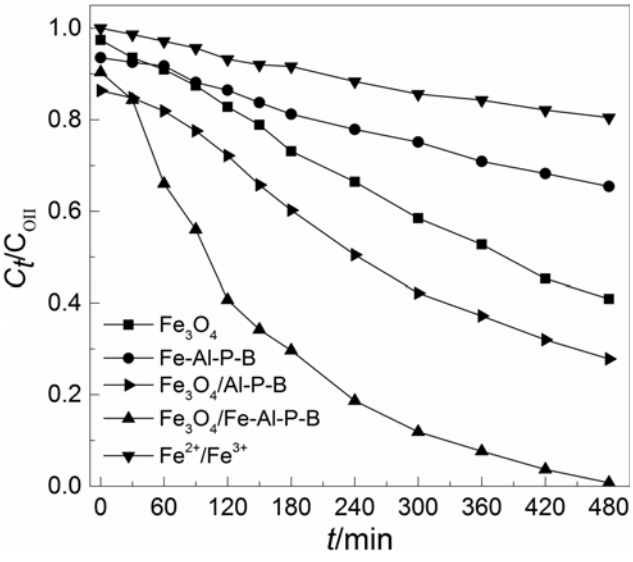

Fig. 7. Degradation of Orange II using different catalysts (C_{OII}=0.23 mmol·L^{-1}, 10 mmol·L^{-1} of H_2O_2, 0.5 g·L^{-1} of Fe_3O_4 or Al-Fe-P-B, 1.0 g·L^{-1} of Fe_3O_4/Al-Fe-P-B, pH=4, 40 °C).

between dye molecules and surfaces of magnetite, promoting the formation of metal oxide-pollutant inner-sphere complexes, which has an advantage to the degradation of pollutants [9,34]. Moreover, in Fig. 6 all the degradation processes also comply with pseudo-first-order rate law.

2-5. The Synergistic Effect between Fe_3O_4 and Al-Fe-P-B

To compare with the past system [27], the removal rates of OII by Fe_3O_4/Al-P-B and Fe_3O_4/Al-Fe-P-B in the same reaction condition are shown in Fig. 7. Before the addition of H_2O_2, the removal of OII only relies on adsorption. It can be seen that the removal rates of Fe_3O_4/Al-P-B and Fe_3O_4/Al-Fe-P-B just by adsorption are 14.1% and 9.6%, respectively. Since the specific surface area of

Fe_3O_4/Al-P-B (103.83 $m^2 g^{-1}$) in previous study is higher than that of Fe_3O_4/Al-Fe-P-B (53.02 $m^2 g^{-1}$), and the average size of Fe_3O_4 nanoparticles is much smaller in Fe_3O_4/Al-P-B, the Fe_3O_4/Al-P-B can be able to adsorb more OII molecules. However, after the addition of H_2O_2, it can be obviously found that the degradation efficiency of OII in the present of Fe_3O_4/Al-Fe-P-B is much higher than that of Fe_3O_4/Al-P-B through heterogeneous Fenton reaction. The enhanced catalytic activity of Fe_3O_4/Al-Fe-P-B may due to the higher stability of Fe_3O_4 nanoparticles which synthesized through precipitation oxidization method (Fig. S1-S3 in supplementary data). Moreover, in our previous study [21], we concluded that the immobilized Fe-ions in Al-Fe-P-B were beneficial for the accessibility of the catalyst to reactants (OII and H_2O_2). Thus, the Al-Fe-P-B can provide more available and effective contact surface areas between reactants and active sites than Al-P-B. The adsorbed OII molecules in the immediate vicinity of immobilized Fe-ions are easily attacked by the generated •OH. Therefore, it is more efficient to use Al-Fe-P-B as supporter. As a result, the catalytic efficiency has improved dramatically in the new system.

To investigate the synergistic effect between Fe_3O_4 and Al-Fe-P-B, a comparison of removal rates of OII by Fe_3O_4, Al-Fe-P-B and Fe_3O_4/Al-Fe-P-B is also shown in Fig. 7. Since the ratio of Fe_3O_4 in Fe_3O_4/Al-Fe-P-B was 50%, the dosages of three catalysts in this experiment were 0.5 g L^{-1} for Fe_3O_4 and Al-Fe-P-B and 1.0 g L^{-1} for Fe_3O_4/Al-Fe-P-B, respectively. As can be seen in Fig. 7, the removal rates of OII by Fe_3O_4 and Al-Fe-P-B alone are 59.1% and 34.6% after 480 min, respectively. When using Fe_3O_4/Al-Fe-P-B, the removal rate can reach 99.3%. It can be observed that Fe_3O_4/Al-Fe-P-B is much more efficient than bare Fe_3O_4 or Al-Fe-P-B. On the other hand, the calculated apparent pseudo-first-order rate constants of Fe_3O_4, Al-Fe-P-B and Fe_3O_4/Al-Fe-P-B are 0.0019, 0.0008 and 0.0067 min^{-1} (R^2>0.99), respectively. The degradation efficiency of OII on Fe_3O_4/Al-Fe-P-B is more than the summation of bare Fe_3O_4 and Al-Fe-P-B. Thus, there may be a synergistic effect between Fe_3O_4 and Al-Fe-P-B. Most authors considered that the synergistic effect resulting by the adsorption property of support caused the difference in the rate of substrate degradation [14,15]. In this study, the adsorption capacity of Fe_3O_4/Al-Fe-P-B is enhanced dramatically compared with that of bare Fe_3O_4, which corresponds to the specific surface area (4.68 $m^2 g^{-1}$ for Fe_3O_4 and 53.02 $m^2 g^{-1}$ for Fe_3O_4/Al-Fe-P-B) of these two catalysts. It means that more dye molecules can be absorbed on the surface of Fe_3O_4/Al-Fe-P-B than bare Fe_3O_4. The •OH generated from the surface reaction between H_2O_2 and Fe_3O_4 or Al-Fe-P-B may preferentially react with the surface sorbed OII. The enhanced adsorption of OII has a dramatic promotion of its degradation. A similar effect was found by Ramirez et al. [35] that OII adsorption on carbon support had positive effect on degradation. On the other hand, the dispersity of Fe_3O_4 nanoparticles was improved after immobilized on Al-Fe-P-B, which can be concluded from the SEM photograph and specific surface area. More active sites of Fe_3O_4 nanoparticles are exposed, which results in an increase of the generation of •OH. Thus, the OII molecules are effectively decomposed through an adsorption-degradation synergistic process on the surface of Fe_3O_4/Al-Fe-P-B. The degradation process of OII will be discussed in the next section.

The comparison between Fe_3O_4/Al-Fe-P-B and other type of catalyst commonly used in the similar process is listed in Table 1. As can be seen, the performance of Fe_3O_4/Al-Fe-P-B is fairly good in comparison to that reported before. Further, there are some distinctive advantages of the novel catalyst over other types, such as low cost, simple synthetic method, environment-friendly and, most important of all, easy to be separated with a magnet. Therefore, Fe_3O_4/Al-Fe-P-B could be employed as peroxidase mimetic for removal of OII or other organic pollutant in the present of H_2O_2. With the advantages mentioned above, the novel catalyst may be able to synthesize in a large-scale, which has a huge potential application in the treatment of practical industrial wastewater.

Table 1. Degradation efficiency of OII on various catalysts at similar reaction condition (pH=4, reaction time=5 h)

Catalysts	Degradation efficiency (%)	Reference
Montmorillonite KSF	77.4	[29]
Vanadium-titanium magnetite	30.0	[34]
Carbon-Fe	53.2	[35]
Fe-saponite	51.7	[36]
Zeolite Y-Fe	80.5	[37]
Fe_3O_4/Al-P-B	58.7	[21]
Fe_3O_4/Al-Fe-P-B	88.2	Present work

The processes with heterogeneous Fenton catalysts do not only rely on the reactions that occur on the surface of the catalyst, but also on homogeneous reactions in the bulk phase by dissolved iron released from the catalyst [15]. Hence, a special experiment was conducted to investigate the contribution from the homogeneous Fenton reaction. After the heterogeneous degradation experiment, the reaction solution was filtered through a Millipore filter (pore size 0.22 μm) to remove the solid catalysts. Then H_2O_2 and OII were added to the filtrate, to build a homogeneous Fenton reaction system catalyzed by dissolved iron, which is shown in Fig. 7. The removal rate of OII through homogeneous Fenton reaction is below 20% after 480 min. It can be observed that the effect of homogeneous Fenton reaction on the degradation process can be neglected. The whole degradation of OII by Fe_3O_4/Al-Fe-P-B is dominated by heterogeneous Fenton reaction.

2-6. The Degradation Process of OII

The OII could be removed efficiently under the optimum reaction conditions. However, it is well accepted that some achromatic medium products, which may have higher toxicity than OII itself, will generate during the degradation process. In the treatment of industrial organic wastewater, the chemical oxygen demand (COD) of the effluent quality is an important indicator. The OII and COD_{Cr} removal rates during the degradation process have been recorded as shown in Fig. 8. As can be seen, the COD_{Cr} removal of OII is much slower than its decomposition. Eight hours after the reaction starts the COD_{Cr} removal rate of OII is about 92.2%. But at the same time the decomposition of OII is nearly 100%. So it could be inferred that some achromatic medium products have not been fully degraded.

To investigate the degradation products, the UV-Vis spectra recorded during the degradation of OII are shown in Fig. 9. The azo-dye is characterized by nitrogen to nitrogen bond (-N=N-), and the

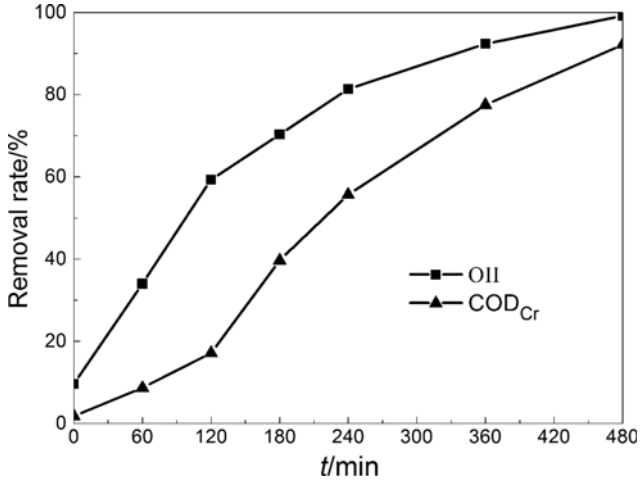

Fig. 8. OII removal rate and COD_{Cr} elimination in the OII degradation (C_{OII}=0.23 mmol·L^{-1}, 10 mmol·L^{-1} of H_2O_2, 1.0 g·L^{-1} of catalyst, pH=4, 40 °C).

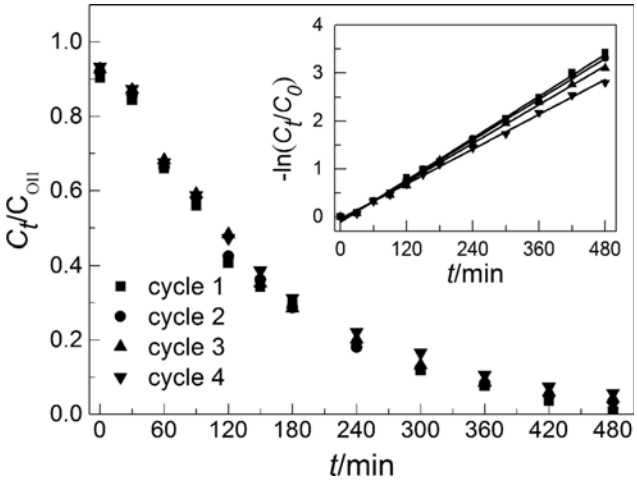

Fig. 10. Effect of recycling the catalyst on the degradation of Orange II (C_{OII}=0.23 mmol·L^{-1}, 10 mmol·L^{-1} of H_2O_2, 1.0 g·L^{-1} of catalyst, pH=4, 40 °C).

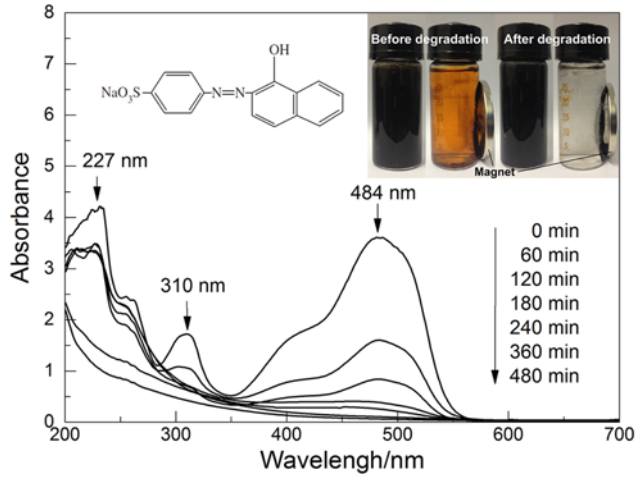

Fig. 9. UV-vis spectra of Orange II as a function of reaction time.

absorption at 484 nm is due to the color of OII solution. The absorption peaks in the ultraviolet region at 227 nm and 310 nm are ascribed to the benzene ring and naphthalene ring, respectively [29]. The results show that the intensity of the 484 nm absorption peak decreases rapidly with the reaction proceeding, indicating that the •OH radical first attacks azo groups and destructs the -N=N- bond. And the intensity of the 227 nm and 310 nm absorption peaks gradually decreases, which implies that these two rings are gradually broken. It confirms the fact that -N=N- bond is easier to destruct than aromatic rang structure and also explains why the COD_{Cr} removal of OII is much slower than its decomposition. However, these absorption peaks did not completely disappear, related to the uncompleted destruction of some aromatic group, which well corresponds to the COD_{Cr} result.

3. The Reusability and Stability of Fe_3O_4/Al-Fe-P-B

The reusability of the catalyst has been evaluated under the reaction conditions which were identical with the first oxidation cycle. After each recycling, the catalyst was treated by magnetic separation, dried and reused. The OII degradation performance on the reused catalyst showed a slight difference with the first oxidation cycle. As shown in Fig. 10, the degradation efficiencies of OII are 99.3%, 96.7%, 95.8% and 94.3% after 480 min for cycle 1, 2, 3 and 4, respectively. All four cycles comply with the pseudo-first-order rate law. It indicates that Fe_3O_4/Al-Fe-P-B has a good long-term reusability and activity. The small decrease of catalytic activity is due to the dissolution of iron.

The XRD pattern and Raman spectra of the Fe_3O_4/Al-Fe-P-B samples before and after use during the OII degradation are presented in Fig. S6 in supplementary data. It can been seen that there are no obvious change of characteristic peaks before and after oxidation reactions in both XRD pattern and Raman spectra, and the SEM image of the used catalyst is also found to be similar to that of the fresh particles (Fig. 1), which further supports the high stability of Fe_3O_4/Al-Fe-P-B. The structural stability of Fe_3O_4 loading on Al-Fe-P-B and the low iron leaking contribute to the stability of the catalytic activity during oxidation reactions. Therefore, the Fe_3O_4/Al-Fe-P-B composite is a stable catalyst with long-term reusability and activity.

CONCLUSION

A novel heterogeneous Fenton catalyst Fe_3O_4/Al-Fe-P-B has been successfully prepared by means of in situ growth of spherical-like Fe_3O_4 nanoparticles on Al-Fe pillared bentonite surface through precipitation oxidization method. The Fe_3O_4/Al-Fe-P-B can be used as an efficient heterogeneous catalyst to degrade Orange II in aqueous solution by Fenton-like reaction. The COD_{Cr} removal rate of OII is about 92.2% 8 h after the degradation started. The whole degradation process follows pseudo-first-order rate law and mainly occurs on the surface of the catalyst. The enhanced catalytic activity of Fe_3O_4/Al-Fe-P-B in heterogeneous Fenton system is due to the synergistic effect between Al-Fe-P-B and Fe_3O_4. The Fe_3O_4/Al-Fe-P-B can achieve solid-liquid separation easily by sample magnetic separation. The novel catalyst has a good reusability and sta-

bility, which will be of potential application in mimicking enzyme catalysis for removal of environmental contaminants.

ACKNOWLEDGEMENTS

This project was supported in part by the Natural Science Foundation of Hubei Province (No. 2014CFB810), Specialized Research Fund for the Doctoral Program of Higher Education of China (20114219110002) and Key Scientific Research Project on Natural Science of Educational Commission of Hubei Province (D20131107).

SUPPORTING INFORMATION

Additional information as noted in the text. This information is available via the Internet at http://www.springer.com/chemistry/journal/11814.

REFERENCES

1. K. Dutta, S. Mukhopadhyay, S. Bhattacharjee and B. Chaudhuri, *J. Hazard. Mater.*, **B84**, 57 (2001).
2. G. Pliego, J. A. Zazo, J. A. Casas and J. J. Rodriguez, *J. Hazard. Mater.*, **252-253**, 180 (2013).
3. L. Xu and J. Wang, *J. Hazard. Mater.*, **186**, 256 (2011).
4. J. Feng, X. Hu and P. L. Yue, *Environ. Sci. Technol.*, **38**, 269 (2004).
5. R. Matta, K. Hanna and S. Chiron, *Sci. Total Environ.*, **385**, 242 (2007).
6. L. Gao, J. Zhuang, L. Nie, J. Zhang, Y. Zhang, N. Gu, T. Wang, J. Feng, D. Yang, S. Perrett and X. Yan, *Nat. Nanotechnol.*, **2**, 577 (2007).
7. J. Zhang, J. Zhuang, L. Gao, Y. Zhang, N. Gu, J. Feng, D. Yang, J. Zhu and X. Yan, *Chemosphere*, **73**, 1524 (2008).
8. S. Zhang, X. Zhao, H. Niu, Y. Shi, Y. Cai and G. Jiang, *J. Hazard. Mater.*, **167**, 560 (2009).
9. L. Xu and J. Wang, *Appl. Catal. B: Environ.*, **123-124**, 117 (2012).
10. S. P. Sun and A. T. Lemley, *J. Mol. Catal. A-Chem.*, **349**, 71 (2011).
11. N. Wang, L. Zhu, M. Wang, D. Wang and H. Tang, *Ultrason. Sonochem.*, **17**, 78 (2010).
12. N. Wang, L. Zhu, D. Wang, M. Wang, Z. Lin and H. Tang, *Ultrason. Sonochem.*, **17**, 526 (2010).
13. M. H. Do, N. H. Phan, T. D. Nguyen, T. T. S. Pham, V. K. Nguyen, T. T. T. Vu and T. K. P. Nguyen, *Chemosphere*, **85**, 1269 (2011).
14. X. Hu, B. Liu, Y. Deng, H. Chen, S. Luo, C. Sun, P. Yang and S. Yang, *Appl. Catal. B: Environ.*, **107**, 274 (2011).
15. J. Chun, H. Lee, S. H. Lee, S. W. Hong, J. Lee, C. Lee and J. Lee, *Chemosphere*, **89**, 1230 (2012).
16. S. Shin, H. Yoon and J. Jang, *Cataly. Commun.*, **10**, 178 (2008).
17. Y. S. Shin, S. G. Oh and B. H. Ha, *Korean J. Chem. Eng.*, **20**, 77 (2003).
18. S. Mnasri-Ghnimi and N. Frini-Srasra, *Korean J. Chem. Eng.*, **32**, 68 (2015).
19. N. Ksontini, W. Najjar and A. Ghorbel, *J. Phys. Chem. Solids*, **69**, 1112 (2008).
20. M. Luo, D. Bowden and P. Brimblecombe, *Appl. Catal. B: Environ.*, **85**, 201 (2009).
21. D. Wan, G. H. Wang, W. B. Li, K. Chen and G. Shu, *Acta Phys.-Chim. Sin.*, **29**, 2429 (2013).
22. L. C. A. Oliveira, R. V. R. A. Rios, J. D. Fabris, K. Sapag, V. K. Garg and R. M. Lago, *Appl. Clay Sci.*, **22**, 169 (2003).
23. P. Yuan, M. Fan, D. Yang, H. He, D. Liu, A. Yuan, J. Zhu and T. Chen, *J. Hazard. Mater.*, **166**, 821 (2009).
24. S. Hashemian and H. Saffari, *Asian J. Chem.*, **23**, 2815 (2011).
25. I. Larraza, M. López-Gónzalez, T. Corrales and G. Marcelo, *J. Colloid Interf. Sci.*, **385**, 24 (2012).
26. L. Lian, X. Cao, Y. Wu, D. Sun and D. Lou, *Appl. Surf. Sci.*, **289**, 245 (2014).
27. G. H. Wang, Y. Z. Lu, W. B. Li, X. Q. Liu and M. D. Sun, *Adv. Mater. Res.*, **581-582**, 292 (2012).
28. X. Xue, K. Hanna and N. Deng, *J. Hazard. Mater.*, **166**, 407 (2009).
29. L. Chen, C. Deng, F. Wu and N. Deng, *Desalination*, **281**, 306 (2011).
30. M. Neamțu, C. Zaharia, C. Catrinescu, A. Yediler, M. Macoveanu and A. Kettrup, *Appl. Catal. B: Environ.*, **48**, 287 (2004).
31. Y. Liu, W. Jiang, Y. Wang, X. J. Zhang, D. Song and F. S. Li, *J. Magn. Magn. Mater.*, **321**, 408 (2009).
32. R. L. Frost and L. Rintoul, *Appl. Clay Sci.*, **11**, 171 (1996).
33. S. Tiwari, D. M. Phase and R. J. Choudhary, *Appl. Phys. Lett.*, **93**, (2008).
34. X. Liang, Y. Zhong, S. Zhu, J. Zhu, P. Yuan, H. He and J. Zhang, *J. Hazard. Mater.*, **181**, 112 (2010).
35. J. H. Ramirez, F. J. Maldonado-Hódar, A. F. Pérez-Cadenas, C. Moreno-Castilla, C. A. Costa and L. M. Madeira, *Appl. Catal. B: Environ.*, **75**, 312 (2007).
36. J. H. Ramirez, C. A. Costa, L. M. Madeira, G. Mata, M. A. Vicente, M. L. Rojas-Cervantes, A. J. López-Peinado and R. M. Martín-Aranda, *Appl. Catal. B: Environ.*, **71**, 44 (2007).
37. M. L. Rache, A. R. García, H. R. Zea, A. M. T. Silva, L. M. Madeira and J. H. Ramírez, *Appl. Catal. B: Environ.*, **146**, 192 (2014).

Supporting Information

Heterogeneous Fenton degradation of Orange II by immobilization of Fe_3O_4 nanoparticles onto Al-Fe pillared bentonite

Wenbing Li[*,,†], Dong Wan[*,†], Guanghua Wang[*,**], Kun Chen[*], Qin Hu[*], and Lulu Lu[*]**

*College of Chemical Engineering and Technology, Wuhan University of Science and Technology, Wuhan 430081, China
**Hubei Coal Conversion and New Carbon Materials Key Laboratory, Wuhan 430081, China
(*Received 28 November 2014 • accepted 4 January 2016*)

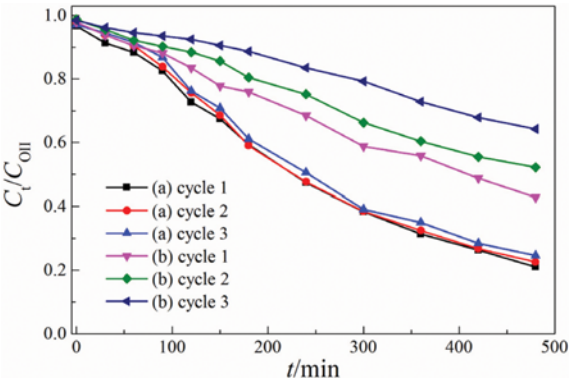

Fig. S1. Effect of recycling the Fe_3O_4 nanoparticles on the degradation of Orange II (C_{OII}=0.23 mmol·L^{-1}, 10 mmol·L^{-1} of H_2O_2, 1.0 g·L^{-1} of Fe_3O_4, pH=4, 40 °C).
(a) Precipitation oxidization method, (b) co-precipitation method

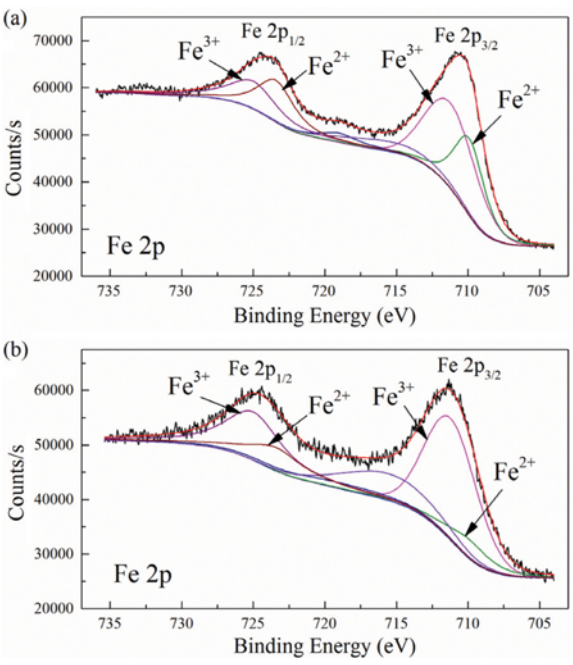

Fig. S2. XPS spectrum of Fe on Fe_3O_4 nanoparticles surface synthesized by precipitation oxidization method (a) and co-precipitation method (b) after degradation of OII (Fe 2p line).

The Fe 2p peaks at binding energies (BE) of 711.2 and 725.0 eV with a satellite signal at 719.0 eV are characteristic of Fe^{3+}, while the peaks at BE of 709.9 and 723.4 eV with a satellite signal at 715.5 eV are characteristic of Fe^{2+}. The components of two oxidation states

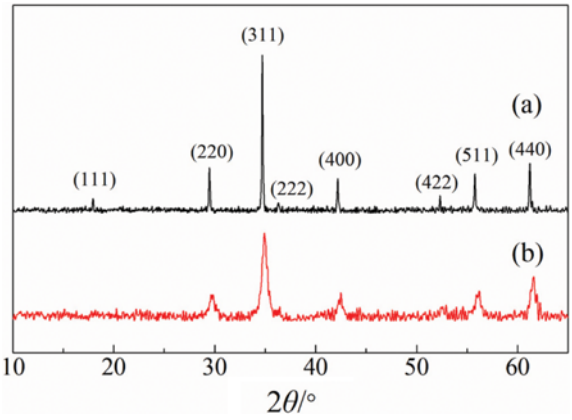

Fig. S3. The XRD patterns of Fe_3O_4 nanoparticles synthesized by precipitation oxidization method (a) and co-precipitation method (b).

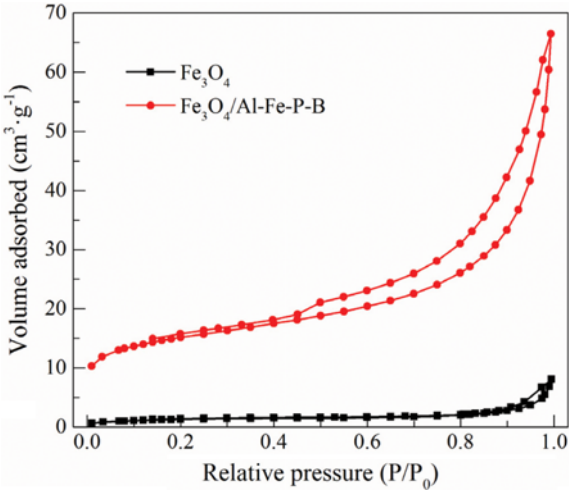

Fig. S4. Nitrogen adsorption/desorption isotherms for Fe_3O_4 and Fe_3O_4/Al-Fe-P-B.

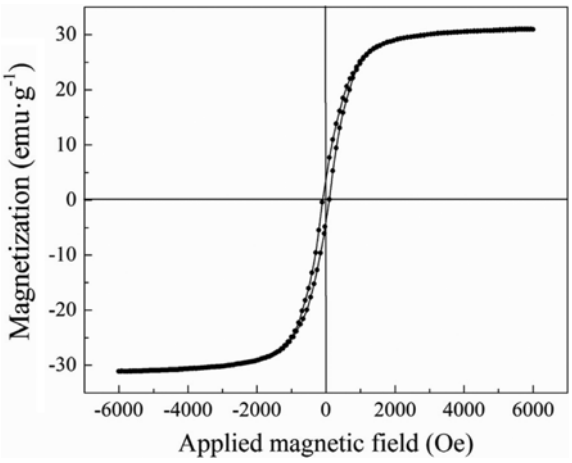

Fig. S5. Hysteresis loop of Fe_3O_4/Al-Fe-P-B.

of surface iron species are consistent with the binding energy values. In Fig. S1(a), the major component is found to be Fe^{3+} which contributes to 69.6% of the total iron surface atoms, while 30.4% of the total iron surface atoms are in the Fe^{2+} state. For the sample synthesized by co-precipitation method, the Fe^{2+} was found to be 3.8% and Fe^{3+} 96.2%, indicating that the outermost surface of Fe_3O_4 nanoparticles is already oxidized.

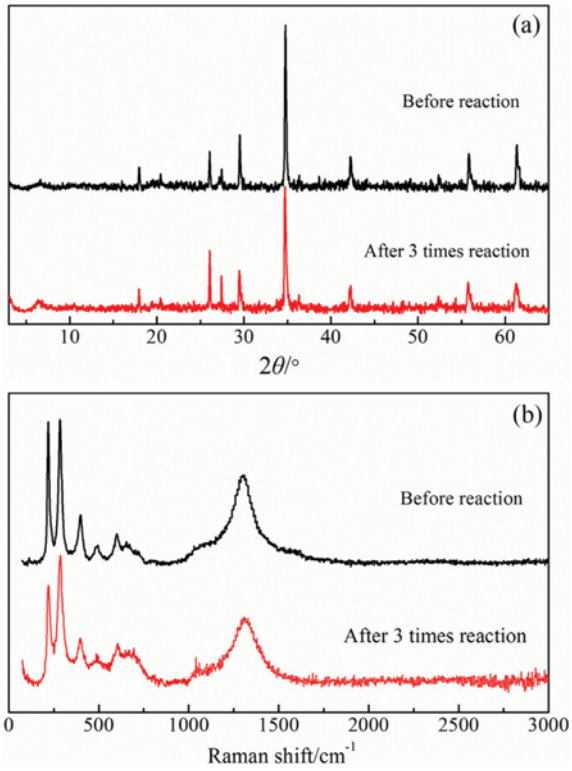

Fig. S6. The XRD pattern (a) and raman spectra (b) of Fe_3O_4/Al-Fe-P-B before and after using.